

Field-tuned skyrmion crystals and anomalous quantum oscillations in magnetic metals

Sopheak Sorn,¹ Stefan Divic,¹ and Arun Paramakanti^{1,*}

¹*Department of Physics, University of Toronto, Toronto, Ontario, Canada M5S 1A7.*

(Dated: March 21, 2025)

Skyrmions are topological magnetic swirls which have been discovered in a variety of itinerant magnets. They are stabilized by anisotropic exchange interactions induced by relativistic spin-orbit coupling. Recent activity in this field has focused on the Berry-flux-induced topological Hall effect in ferromagnetic (FM) skyrmion crystals, and on the hunt for skyrmions and skyrmion crystals in frustrated antiferromagnets. In this work, we study the impact of quartic spin interactions in such systems, and find that it can lead to strong mode-mode coupling which depends on an applied Zeeman magnetic field. This effect combined with the anisotropic exchange couplings leads to the formation of triple-**Q** skyrmion crystals which are shown to have a field-tunable lattice constant. We discuss this effect in triangular-lattice ferromagnets with broken inversion symmetry, which host Dzyaloshinskii-Moriya interactions, as well as in frustrated antiferromagnets such as Gd_2PdSi_3 which have been explored in recent experiments. For FM skyrmion crystals, we show that coupling itinerant electrons to this spin texture leads to a tunable Hofstadter-type model, resulting in Chern bands which strongly depend on a Zeeman field coupled to the local moments. Such magnetic metals are argued to be candidates for observing Zeeman-field-induced anomalous quantum oscillations.

Skyrmions were originally introduced in particle physics as spatially localized and topologically nontrivial field configurations to model nucleons [1]. In recent years, skyrmions have been proposed to occur and observed as spin textures in diverse condensed-matter settings: quantum Hall systems [2–5], bulk and thin film magnets [6–20], and artificially engineered magnetic multilayers [21–23] and oxide interfaces [24–26]. The driving forces for skyrmion formation in the latter systems are anisotropic exchange interactions which favor spin twisting; these are typically induced by broken inversion symmetry and spin-orbit coupling (SOC). The emerging field of “skyrmionics” aims to create and manipulate skyrmions as stable memory units [27–31].

In many of these solid-state materials, such as MnSi, skyrmions occur in crystalline form — as periodic noncoplanar textures obtained by superposing multiple spin spirals [6, 7, 9–12, 17, 32] created by the Dzyaloshinskii-Moriya (DM) exchange interaction which is present in noncentrosymmetric systems [33, 34]. An electron moving in such a spin texture picks up a Berry phase [35–37]. The resulting Berry flux, arising from the scalar spin chirality of the skyrmion crystal, modifies the conventional Hall effect due to an orbital magnetic field, leading to an observed “topological Hall effect” contribution [16, 32, 38]. Remarkably, this suggests that, under suitable circumstances, even a pure Zeeman magnetic field, which couples to the local moments but not directly to the orbital motion of the electrons, might lead to analogues of quantum oscillations, conventionally attributed to Landau quantization in an orbital magnetic field.

More recently, skyrmion crystals have been discovered in a metallic antiferromagnet Gd_2PdSi_3 [39]. In this systems, the spiral magnetism appears to be favored by frus-

trated Gd-Gd magnetic exchange couplings on a triangular lattice. In general, such frustrated antiferromagnets might support stronger spin twisting and thus a large scalar spin chirality [40, 41]. Indeed, transport experiments on Gd_2PdSi_3 have found a large topological Hall effect attributed to a skyrmion crystal at intermediate field strength [39]. On the theoretical front, studies of doped triangular-lattice Hubbard and Kondo models [42, 43] have discovered a noncoplanar AFM spin crystal formed from superposing period-2 AFM stripes, which supports a quantized $\sigma_{xy} = e^2/h$.

Motivated by these observations, we explore skyrmion crystals in a two-dimensional (2D) triangular lattice, and study the effect of a Zeeman magnetic field on the spin textures, and the impact of such spin textures on the electronic bands. Using a microscopic spin model with compass and DM exchange interactions, we show that a symmetry-allowed quartic anisotropy can induce strong mode-mode coupling between the spiral spin modes and the uniform magnetization mode. In the presence of a Zeeman field, this mode coupling tunes the spiral wavevectors due to an effective renormalization of the quadratic single-ion anisotropy. We show that this interplay results in an enhancement of the skyrmion regime. Crucially, we show this leads to skyrmion lattices which are highly field-tunable; for the 3D multiferroic cubic crystal Cu_2OSeO_3 [18], this has also been recently reported and discussed within Landau theory [44].

In systems with dominant FM couplings and DM interactions, we find a field-induced Néel skyrmion crystal. Increasing the Zeeman field in this skyrmion crystal leads to a decrease in the magnitude of the spiral wavevector, resulting in an expansion of the skyrmion lattice. For the case with inversion symmetry (no DM interactions) and frustrating AFM couplings, we find that the Zeeman field leads to an increase in the spiral wavevector magnitude, together with an intermediate Bloch skyrmion-crystal phase, as recently observed in Gd_2PdSi_3 [39].

*Electronic address: arunp@physics.utoronto.ca

In the FM case, a computation of the band structures of electrons Kondo coupled to this tunable spin texture reveals the formation of Chern bands. At low energies, we find isolated bands with Chern number $C = -1$, while at high energies we discover pairs of bands carrying a total Chern number $C_{\text{pair}} = -2$ which feature band-sticking along high symmetry directions in the Brillouin zone. Due to the field-tuning of the skyrmion lattice, we show that even a purely Zeeman magnetic field acting on the local moments leads to anomalous quantum oscillations in the electronic density of states. This should manifest in various physical observables, e.g., the electronic specific heat and transport of such skyrmion metals.

Model Hamiltonian. — We begin with a Hamiltonian describing classical spins on a triangular lattice, which has the key ingredients previously shown to stabilize 2D skyrmion crystals within a Landau theory [14, 24, 25]:

$$H_0 = \frac{1}{2} \sum_{i,j} J_{ij} \mathbf{S}_i \cdot \mathbf{S}_j + D \sum_{\langle ij \rangle} (\hat{z} \times \hat{r}_{ij}) \cdot (\mathbf{S}_i \times \mathbf{S}_j) - A_c \sum_{\langle ij \rangle} (\mathbf{S}_i \cdot (\hat{z} \times \hat{r}_{ij})) (\mathbf{S}_j \cdot (\hat{z} \times \hat{r}_{ij})) - \mathcal{B} \sum_i S_{iz}. \quad (1)$$

Here J_{ij} is the Heisenberg exchange; we may choose $J_{ij} < 0$ as appropriate for a ferromagnet, or $J_{ij} > 0$ to represent a frustrated antiferromagnet. SOC induces two important anisotropic exchange interactions: A_c is a compass term which is symmetry-allowed even in the presence of inversion symmetry, while D is the chiral Rashba DM interaction [33, 34, 45, 46] which arises only when $\hat{z} \rightarrow -\hat{z}$ inversion symmetry is broken. Dresselhaus DM interaction however is not allowed by vertical-plane reflections σ_v of the triangular lattice. The Zeeman field \mathcal{B} allows for control of the ground state of the system. Increasing \mathcal{B} leads to a transition from single-mode spiral order to a triple- \mathbf{Q} skyrmion crystal, and eventually to a polarized ferromagnet at large \mathcal{B} [24, 47]. We supplement H_0 with two terms

$$H_1 = A_s \sum_i S_{iz}^2 + \lambda_{\perp} \sum_i S_{iz}^4 \quad (2)$$

Here A_s is a single-ion anisotropy which has been previously shown to influence the stability of skyrmion-crystal order [8, 14, 24, 47, 48]. The ingredient we focus on here is the local anisotropy $\lambda_{\perp} > 0$ which is the single non-trivial *quartic* coupling allowed by the C_{6v} symmetry of the lattice. As discussed below, this term leads to strong mode-mode coupling and field-tunable skyrmion lattices.

To study the ground states of the Hamiltonian $H_0 + H_1$, we resort to a variational approach. We begin by imposing the spin-length constraint $\mathbf{S}_i^2 = 1$ on average, setting $\sum_i \mathbf{S}_i^2 = N$ where N is the number of sites. For $\lambda_{\perp} = \mathcal{B} = 0$, a Luttinger-Tisza analysis yields degenerate spin-spiral solutions. We therefore consider a general ansatz $\mathbf{S}_i = \mathbf{m}_0 + \sum_n \mathbf{m}_n e^{i\mathbf{Q}_n \cdot \mathbf{r}_i}$, retaining the uniform component \mathbf{m}_0 , and a set of symmetry-equivalent spirals with wavevectors \mathbf{Q}_n and amplitudes \mathbf{m}_n .

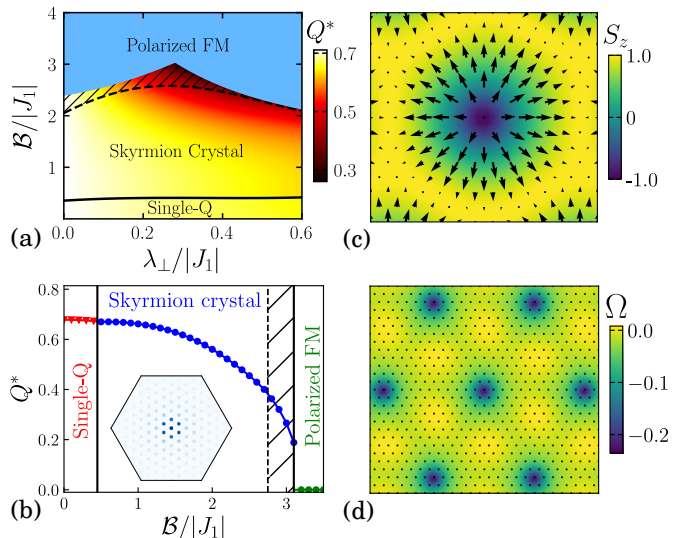


FIG. 1: (a) Phase diagram of the triangular ferromagnet with DM interaction as a function of λ_{\perp} and \mathcal{B} showing topologically trivial single- \mathbf{Q} spiral and FM phases, and nontrivial triple- \mathbf{Q} skyrmion-crystal phase. We have fixed $D = |J_1|$, $A_c = 0.4|J_1|$ and $A_s = 0.5|J_1|$. Color scale shows optimal momentum Q^* in different regimes. Hatched region indicates a triple- \mathbf{Q} regime where the core spins have flipped from negative to positive magnetization before entering the polarized FM phase. This phase has a trivial total Berry flux, but is unstable after we keep a large number of harmonics and impose the hard constraint $\mathbf{S}_i^2 = 1$. (b) Field dependence of Q^* , at a fixed $\lambda_{\perp} = 0.3$, displaying strong variation in the skyrmion-crystal phase. The inset shows the intensity plot of the spin structure factor inside the first Brillouin zone for a typical skyrmion crystal, featuring peaks at the center $\mathbf{Q} = 0$, the primary triple- \mathbf{Q} wavevectors and higher harmonics. (c) Structure of the Néel skyrmion with negative magnetization at the core. (d) Spatial variation of solid angle Ω subtended by three noncoplanar spins on elementary triangular plaquettes. $\Omega/4\pi$ sums to a topological charge (-1) per skyrmion.

The simplest skyrmion lattice is constructed from a set of three primary spiral wavevectors which sum to zero (in addition to the FM mode), i.e. it is a triple- \mathbf{Q} spin crystal. The impact of the hard-spin constraint and the nonlinear coupling $\lambda_{\perp} \neq 0$ is to generate higher harmonics of these primary \mathbf{Q} 's [11]. The full variational state is obtained from an optimal ansatz for $\{\mathbf{m}_0, \mathbf{m}_n, \mathbf{Q}_n\}$ (cutoff at a certain order in the harmonics), followed by explicitly normalizing the spin vector at each site (see Supplemental Material for details).

Ferromagnet with DM interactions. — We begin with the case of a ferromagnet with broken inversion symmetry, setting $J_{ij} = J_1 < 0$ for nearest-neighbor FM exchange, and $A_c, D \neq 0$. The resulting phase diagram, upon tuning \mathcal{B} and λ_{\perp} , is depicted in Fig. 1(a). For $\lambda_{\perp} = 0$, this is consistent with previous studies, exhibiting spiral, skyrmion crystal, and FM phases with increasing \mathcal{B} [24]. Our key observation is that incorporating $\lambda_{\perp} \neq 0$ leads to a qualitatively similar phases. The key

difference is that the primary wavevectors \mathbf{Q}^* , which lie in the Γ - M directions, now exhibit a strong field dependence, as seen from Fig. 1(b). This leads to a strong field dependence of the skyrmion-crystal lattice constant. We trace this dependence of \mathbf{Q}^* on \mathcal{B} to an effective renormalization of the easy-plane anisotropy. This is heuristically seen from a Hartree-level treatment [44] of the λ_{\perp} quartic term, which yields $A_s^{\text{eff}} = A_s + 6\lambda_{\perp}m_0^2$, where m_0 increases with increasing \mathcal{B} . This renormalization of A_s leads to a change in the optimal \mathbf{Q}^* , thus tuning the skyrmion crystal (see Supplemental Material).

The spin texture stabilized in this system is a lattice of Néel skyrmions as depicted in Fig. 1(c). We find that the solid angle Ω subtended by the three spins on each elementary triangular plaquette shows a strong spatial variation, being higher at the skyrmion core, as seen from Fig. 1(d). (In the continuum, $\Omega = \mathbf{S} \cdot \partial_x \mathbf{S} \times \partial_y \mathbf{S}$.) Adding up $\Omega/4\pi$ across the lattice, we obtain an average topological charge (-1) per skyrmion. When the Zeeman field enhances the skyrmion-crystal lattice constant, this flux gets distributed over a larger area. We thus expect electrons moving in such a spin-textured background to sense an average “emergent orbital field” which decreases as we increase the Zeeman field on the local moments.

Anomalous quantum oscillations. — To study the influence of the skyrmion crystal on conduction electrons, we have diagonalized a Hamiltonian for electrons on the triangular lattice (same lattice as the spins),

$$H_{\text{elec}} = -\sum_{j,\ell} t_{j\ell} c_{j\alpha}^{\dagger} c_{\ell\alpha} - \sum_{j,\ell} i\chi_R^{(j\ell)} c_{j\alpha}^{\dagger} [\hat{z} \times \hat{r}_{j\ell} \cdot \vec{\sigma}]_{\alpha\beta} c_{\ell\beta} - J_H \sum_j \mathbf{S}_j \cdot c_{j\alpha}^{\dagger} \vec{\sigma}_{\alpha\beta} c_{j\beta}. \quad (3)$$

We pick a nearest-neighbor ordinary hopping t and Rashba hopping χ_R , and assume that the electrons sense the underlying spin texture $\{\mathbf{S}_i\}$ via a ferromagnetic Kondo interaction $J_H > 0$ [37, 49, 50] which can physically arise from atomic Hund’s coupling.

The resulting number of electronic bands depends on the skyrmion lattice. If we pick $\mathbf{Q}^* = (4\pi/\sqrt{3})(m/n)\hat{y}$ (and its symmetry-allowed partners) as the best approximant to the optimal spin-crystal wavevector, the periodic “magnetic unit cell” of the triple- \mathbf{Q} state has n^2 triangular lattice sites and encloses m^2 skyrmions. This hosts $2n^2$ bands including spin.

This commensurability effect of the skyrmion lattice with the underlying crystal lattice does not appear in continuum field theories. It also appears not to have been discussed in previous work on lattice models, since these have only studied the simplest example with fixed $m = 1$ [50–52]. Here, and more clearly in the AFM model below, we will see that this more general case results in the Berry flux, and indeed all local observables, exhibiting small modulations from one skyrmion to the next, with periodicity recovered over the magnetic unit cell. Crucially, we find that adding up the solid angles subtended by the three spins on an elementary plaquettes leads to

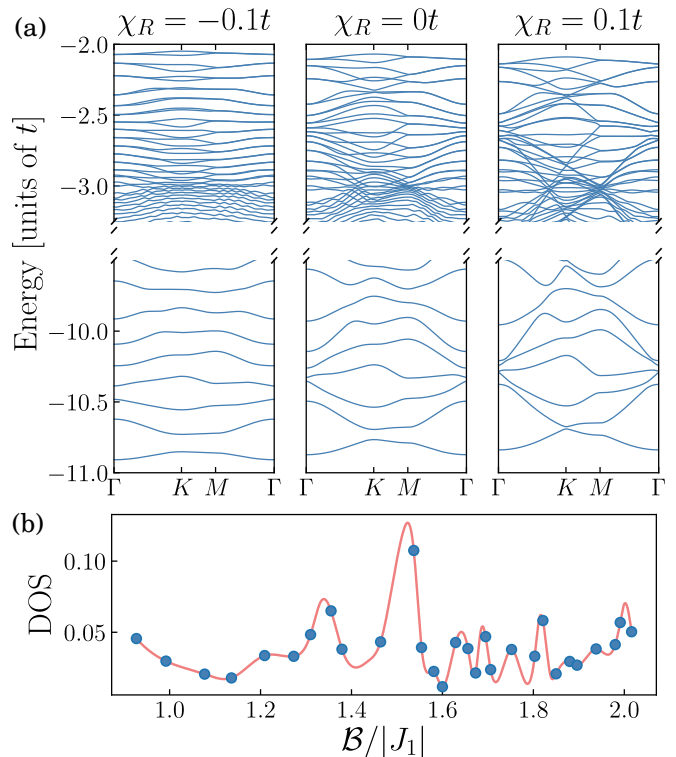


FIG. 2: (a) Band structure along high-symmetry paths in the hexagonal BZ in the skyrmion-crystal phase for the ferromagnet with DM interactions. The conduction electrons are assumed to have ordinary hopping t , a Rashba hopping $\chi_R = 0, \pm 0.1t$, with a coupling to the localized spins via ferromagnetic exchange $J_H/t = 5$. The plotted bands correspond to half of all the bands, where conduction-electron spins are aligned with the local moments. The low-energy bands are well isolated, and carry Chern numbers -1 . The high-energy bands come in pairs, exhibiting band sticking along Γ - M , with total Chern number $C_{\text{pair}} = -2$. Finally, there are a set of bands near $E \approx -3t$ which are connected and carry large $C > 0$ Chern numbers to ensure that the total Chern number is zero. (b) Oscillations in the DOS at the Fermi level (in units of t^{-1}) for $\chi_R = 0$ and fixed conduction electron density $\rho = 0.1$ electrons per site. These anomalous quantum oscillations arise from the \mathcal{B} dependence of \mathbf{Q}^* .

a quantized result, in units of 4π , only when we sum over *all* m^2 skyrmions in the magnetic unit cell. Thus, the topological charge per skyrmion is quantized to (-1) only when averaged over the full magnetic unit cell.

To study the skyrmion-crystal band structure, we have considered magnetic unit cells of up to $n^2 = 3600$ sites with varying \mathcal{B} , and diagonalized the corresponding $2n^2 \times 2n^2$ electronic Hamiltonian at all momenta \mathbf{k} in the reduced hexagonal Brillouin zone (BZ) of the skyrmion crystal. The resulting band dispersions for $\chi_R/t = 0, \pm 0.1$ and $J_H/t = 5$ are shown along high-symmetry paths in the BZ in Fig. 2(a). The plotted bands correspond to half of all the $2n^2$ bands, where conduction-electron spins are aligned with the local mo-

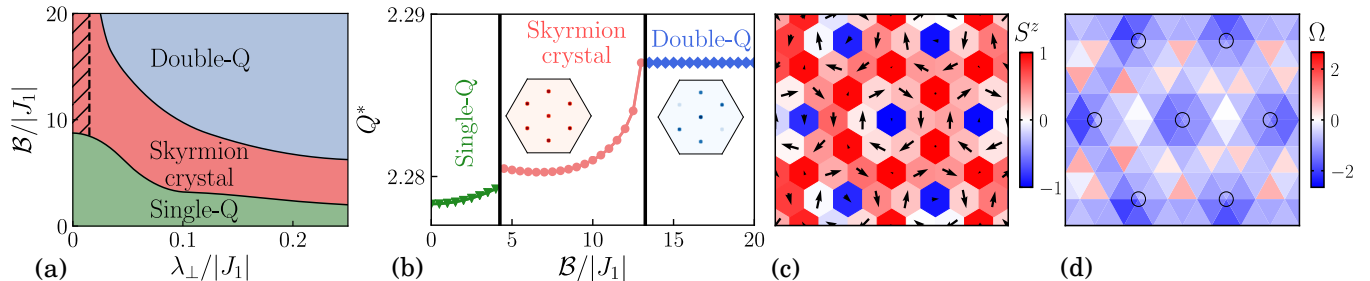


FIG. 3: (a) Phase diagram of the triangular AFM model with compass term as a function of quartic anisotropy λ_{\perp} and field \mathcal{B} for fixed $A_s = -0.25|J_1|$, $A_c = -0.2|J_1|$ and $J_2 = 4|J_1|$. With increasing \mathcal{B} at fixed λ_{\perp} , we find an evolution from single- \mathbf{Q} to a skyrmion crystal to a double- \mathbf{Q} phase. The hatched region is a trivial triple- \mathbf{Q} phase, featuring a triangular array of negative-magnetization islands in a positive-magnetization background, similar to the “bubble crystal” studied in Ref.[53]. (b) Evolution of the wavevector \mathbf{Q}^* with \mathcal{B} . Both (a) and (b) are qualitatively consistent with data on Gd_2PdSi_3 . The insets are typical intensity plots of the spin structure factors inside the first Brillouin zone for the skyrmion crystal phase and the double- \mathbf{Q} phase. (c) Spin texture in the skyrmion-crystal phase, showing Bloch skyrmions (centered on blue hexagons) in a ferromagnetic background. (d) Spatial variation of the solid angle Ω subtended by the three spins on elementary triangular plaquettes; circles denote the skyrmion cores. Summing $\Omega/4\pi$ yields an average topological charge (-1) per skyrmion.

ments. In all cases, these low-energy bands appear isolated and have Chern number $C = -1$, resembling somewhat dispersive Landau levels. Thus, at special electronic densities which fill up an integer number of these bands, we would expect a large quantized topological Hall effect [50–52]. The high-energy bands come in pairs due to band sticking along the high-symmetry Γ - M line; in this case the total Chern number of the pair is $C_{\text{pair}} = -2$. In an intermediate-energy window, around $E/t \approx -3$, we find a set of bands carrying large positive Chern numbers $C \gg 1$, which ensures that the Chern numbers over all bands sum to zero. For $|\chi_R| \ll t$, this occurs around the van-Hove singularity in the density of states (DOS) of the triangular lattice, where a Lifshitz transition occurs near the M -point. This distribution of Chern numbers is analogous to that for the Hofstadter model [51, 52, 54].

Fig. 2(b) plots the electronic DOS at the Fermi level as we vary the Zeeman field \mathcal{B} on the local moments, staying at a fixed electron density $\rho = 0.1$ electrons per site of the original triangular lattice. Despite the low energy Chern bands having some dispersion, we find that the DOS shows clear anomalous quantum oscillations, even though the electrons are not subject to any direct orbital magnetic field! The oscillations can be understood by observing that the expansion of the skyrmion lattice leads to a decrease in the average Berry flux density. This problem is thus analogous to studying a Hofstadter model with a decreasing magnetic flux ϕ per plaquette [54–59]. In the conventional Hofstadter problem, varying ϕ leads to a rich Hofstadter butterfly spectrum due to the interplay of two length scales — set by the unit cell area of the underlying lattice and the area of the magnetic unit cell. In our problem, the role of ϕ is effectively played by $Q^{*2} = [(4\pi/\sqrt{3})(m/n)]^2$. As the Zeeman field \mathcal{B} is tuned, Q^* changes, and the oscillations in the DOS can thus be identified with a scan in ϕ through the Hofstadter butterfly spectrum. Our model however differs

from the conventional Hofstadter model in that the flux per plaquette is not really uniform, and there exists a third length scale — the skyrmion size — which characterizes the spatial inhomogeneity of the emergent “orbital magnetic field”.

These anomalous DOS oscillations should impact all physical observables [58, 60–63]. Since we are tuning the Zeeman field \mathcal{B} on the local moments, this nontrivial effect is *distinct* from previous studies which simply varied the electron filling in a fixed skyrmion texture. The oscillations we describe would be further impacted by the direct Zeeman and orbital effects of the magnetic field on the conduction electrons; however, the typically much stronger effect of the skyrmion lattice and its Berry flux should still lead to observable effects as deviations from conventional quantum oscillations in skyrmion magnets.

Inversion symmetric antiferromagnets. — We next turn to the antiferromagnet Gd_2PdSi_3 , where recent experiments have reported nontrivial spin textures via the discovery of a large topological Hall effect at intermediate applied magnetic fields [39]. Gd_2PdSi_3 has a layered structure with triangular lattices of Gd moments spaced apart by metallic Pd/Si layers. We assume that Pd and Si atoms are distributed homogeneously in the Pd/Si layer; the crystal structure then has inversion symmetry on average about the Gd-Gd bond centers, and we can then set the DM exchange interactions between the Gd moments to zero to simplify our model Hamiltonian [64]. Magnetic resonant X-ray scattering (RXS) [39] has found evidence for incommensurate magnetic order with wavevectors along Γ - M line in the hexagonal BZ. Such ordering could arise from interactions mediated by the conduction electrons.

To understand these observations, we study the Hamiltonian $H_0 + H_1$ from Eqns.1,2, applied to a single triangular Gd layer embedded in the crystal, with FM nearest-neighbor exchange $J_1 < 0$ and large AFM frustrating

next-neighbor exchange $J_2 > 0$. Inversion symmetry leads to the absence of a DM interaction between Gd moments, thus $D = 0$. However, a compass term is permitted, so we set $A_c \neq 0$. Our work goes beyond previous studies of skyrmions in this frustrated magnetic Hamiltonian [40, 41] by incorporating the impact of symmetry-allowed quartic couplings as well as compass terms. As in the FM example, we have examined variational single- \mathbf{Q} and multi- \mathbf{Q} orders for the ground state of this AFM Hamiltonian. We thus arrive at the phase diagram shown in Fig. 3(a). We find in this case that the zero-field single- \mathbf{Q} spiral order gives way to a triple- \mathbf{Q} state with increasing \mathcal{B} , which in turn gives way to a double- \mathbf{Q} state. This sequence of phases is qualitatively consistent with the magnetic RXS results [39]. The eventual polarized ferromagnet appears at much higher fields $\mathcal{B} \gtrsim 30|J_1|$, which has not been accessed in experiments at the lowest temperature. Interestingly, we find that the characteristic wavevector Q^* of the spirals making up the spin texture increases slightly in this case as we increase \mathcal{B} as shown in Fig. 3(b). Precisely such a trend has been observed in Gd_2PdSi_3 [39]. With increasing field, the intensity in the FM component increases, while the intensity in the incommensurate wavevectors decreases.

The real-space spin texture in the intermediate-field triple- \mathbf{Q} state is shown in Fig. 3(c). We find that the crystal is made of Bloch skyrmions in a ferromagnetic background. Fig. 3(d) shows the spatial variation of the solid angle Ω subtended by the three noncoplanar spins on each elementary triangular plaquette, with the circles indicating the cores of the skyrmions. Summing $\Omega/4\pi$ over the magnetic unit cell yields a net topological charge (-1) per skyrmion. In this AFM case, due to the shorter length scale associated with the spin texture, the distinction between the interskyrmion separation and the magnetic unit cell periodicity alluded to earlier is clearly visible in the spatial structure of the texture as well as Ω . For instance, Ω around each skyrmion core has a slightly different pattern, and the periodicity is only recovered at a longer length scale of the magnetic unit cell.

Here, the skyrmion crystal is stabilized by the interplay between the quadratic and the quartic anisotropy terms, A_s and λ_\perp respectively, while a nonzero A_c is needed to get a tunable Q^* . We find $A_c > 0$ favors Néel-type skyrmion crystals, while $A_c < 0$ stabilizes Bloch-type skyrmion crystals; however, only the latter also leads to the observed enhancement of Q^* with field. We thus expect $A_c < 0$, and predict that the experiments should observe a lattice of Bloch skyrmions. More importantly, if we assume $A_c = 0$, the Hamiltonian for this classical spin system has a global symmetry under which we can flip all $S_x \rightarrow -S_x$ or $S_y \rightarrow -S_y$. This operation also flips the skyrmion topological charge [40]. Since the real crystal would then be expected to have equal number of domains of this spontaneously broken symmetry, this

would lead to a zero average topological Hall effect. This is in striking contrast to the observed large topological Hall effect. A nonzero compass exchange term, which explicitly breaks this global spin flip symmetry and selects a specific charge $Q = -1$ for the skyrmion, is thus crucial for observing a nonzero topological Hall effect.

Discussion. — We have studied magnetic skyrmions in 2D FM and AFM systems, arguing that quartic anisotropies can lead to field tunable skyrmion crystals. Such anisotropies can arise from single-ion physics or from integrating out conduction electrons.

For the FM case, where this field tunability is highly pronounced, we have shown that anomalous quantum oscillations can arise from just the impact of a Zeeman field on the local moments. The Chern bands which contribute to these oscillations are already somewhat dispersive; we thus expect disorder broadening which is weaker than the scale of this bandwidth (which is also comparable to the band gap) will not alter our main results. The amplitude of these anomalous oscillations are not expected to follow simple Lifshitz-Kosevich scaling since, unlike Landau levels, the emergent Chern bands are not flat and equispaced in energy. The physics underlying these anomalous quantum oscillations is not crucially dependent on the triangular lattice symmetry - thus, a heterostructure with an ultrathin metallic film deposited on insulating Cu_2OSeO_3 , where a field-tunable skyrmion crystal has been reported [44], may be a potential venue for observing this effect. However, the length scale $1/Q^*$ in bulk Cu_2OSeO_3 is much larger than what we have explored here. Further experimental and theoretical work on such a proposed heterostructure would thus be valuable, in assessing the viability of our proposal, as would searches for more promising material candidates.

For the AFM case, we have found that we can qualitatively understand recent observations of multi- \mathbf{Q} orders reported in Gd_2PdSi_3 crystals. We have shown that the field dependence of the skyrmion wavevector and the subtlety in understanding the experimentally measured large topological Hall effect in the intermediate skyrmion crystal phase can be consistently resolved from the interplay of magnetic frustration and various anisotropies including compass exchange terms. Further work is needed to extract the full set of microscopic Hamiltonian parameters in order to make quantitative contact with experiments on Gd_2PdSi_3 .

We acknowledge extremely useful discussions with Achim Rosch. This research was funded by NSERC of Canada and the Canadian Institute for Advanced Research. Computations were performed on the Niagara supercomputer at the SciNet HPC Consortium. SciNet is funded by: the Canada Foundation for Innovation under the auspices of Compute Canada; the Government of Ontario; Ontario Research Fund - Research Excellence; and the University of Toronto.

-
- [1] T. Skyrme, *Nuclear Physics* **31**, 556 (1962).
- [2] S. L. Sondhi, A. Karlhede, S. A. Kivelson, and E. H. Rezayi, *Phys. Rev. B* **47**, 16419 (1993).
- [3] H. A. Fertig, L. Brey, R. Côté, and A. H. MacDonald, *Phys. Rev. B* **50**, 11018 (1994).
- [4] S. E. Barrett, G. Dabbagh, L. N. Pfeiffer, K. W. West, and R. Tycko, *Phys. Rev. Lett.* **74**, 5112 (1995).
- [5] Y. P. Shkolnikov, S. Misra, N. C. Bishop, E. P. De Poortere, and M. Shayegan, *Phys. Rev. Lett.* **95**, 066809 (2005).
- [6] A. Bogdanov and A. Hubert, *Sov. Phys. JETP* **68**, 101 (1989).
- [7] A. Bogdanov and A. Hubert, *Journal of Magnetism and Magnetic Materials* **138**, 255 (1994).
- [8] A. N. Bogdanov, U. K. Röbner, M. Wolf, and K.-H. Müller, *Phys. Rev. B* **66**, 214410 (2002).
- [9] U. K. Röbner, A. N. Bogdanov, and C. Pfleiderer, *Nature* **442**, 797 EP (2006).
- [10] B. Binz, A. Vishwanath, and V. Aji, *Phys. Rev. Lett.* **96**, 207202 (2006).
- [11] B. Binz and A. Vishwanath, *Phys. Rev. B* **74**, 214408 (2006).
- [12] S. Mühlbauer, B. Binz, F. Jonietz, C. Pfleiderer, A. Rosch, A. Neubauer, R. Georgii, and P. Böni, *Science* **323**, 915 (2009).
- [13] X. Z. Yu, Y. Onose, N. Kanazawa, J. H. Park, J. H. Han, Y. Matsui, N. Nagaosa, and Y. Tokura, *Nature* **465**, 901 EP (2010).
- [14] A. B. Butenko, A. A. Leonov, U. K. Röbner, and A. N. Bogdanov, *Phys. Rev. B* **82**, 052403 (2010).
- [15] S. Heinze, K. von Bergmann, M. Menzel, J. Brede, A. Kubetzka, R. Wiesendanger, G. Bihlmayer, and S. Blügel, *Nature Physics* **7**, 713 EP (2011).
- [16] T. Schulz, R. Ritz, A. Bauer, M. Halder, M. Wagner, C. Franz, C. Pfleiderer, K. Everschor, M. Garst, and A. Rosch, *Nature Physics* **8**, 301 EP (2012).
- [17] A. Tonomura, X. Yu, K. Yanagisawa, T. Matsuda, Y. Onose, N. Kanazawa, H. S. Park, and Y. Tokura, *Nano Letters* **12**, 1673 (2012).
- [18] S. Seki, X. Z. Yu, S. Ishiwata, and Y. Tokura, *Science* **336**, 198 (2012).
- [19] S. Hayami and Y. Motome, *Phys. Rev. Lett.* **121**, 137202 (2018).
- [20] K. N. Okada, Y. Kato, and Y. Motome, *ArXiv e-prints* (2018), 1809.07582.
- [21] W. Jiang, P. Upadhyaya, W. Zhang, G. Yu, M. B. Jungfleisch, F. Y. Fradin, J. E. Pearson, Y. Tserkovnyak, K. L. Wang, O. Heinonen, et al., *Science* **349**, 283 (2015).
- [22] A. S. Ahmed, B. D. Esser, J. Rowland, D. W. McComb, and R. K. Kawakami, *Journal of Crystal Growth* **467**, 38 (2017).
- [23] A. S. Ahmed, J. Rowland, B. D. Esser, S. R. Dunsiger, D. W. McComb, M. Randeria, and R. K. Kawakami, *Phys. Rev. Materials* **2**, 041401 (2018).
- [24] S. Banerjee, J. Rowland, O. Erten, and M. Randeria, *Phys. Rev. X* **4**, 031045 (2014).
- [25] X. Li, W. V. Liu, and L. Balents, *Phys. Rev. Lett.* **112**, 067202 (2014).
- [26] J. Matsuno, N. Ogawa, K. Yasuda, F. Kagawa, W. Koshibae, N. Nagaosa, Y. Tokura, and M. Kawasaki, *Science Advances* **2** (2016).
- [27] A. Fert, V. Cros, and J. Sampaio, *Nature Nanotechnology* **8**, 152 EP (2013).
- [28] N. Nagaosa and Y. Tokura, *Nature Nanotechnology* **8**, 899 EP (2013).
- [29] A. K. Yadav, C. T. Nelson, S. L. Hsu, Z. Hong, J. D. Clarkson, C. M. Schlepütz, A. R. Damodaran, P. Shafer, E. Arenholz, L. R. Dedon, et al., *Nature* **530**, 198 EP (2016).
- [30] W. Jiang, G. Chen, K. Liu, J. Zang, S. G. te Velthuis, and A. Hoffmann, *Physics Reports* **704**, 1 (2017), skyrmions in Magnetic Multilayers.
- [31] A. Hrabec, J. Sampaio, M. Belmeguenai, I. Gross, R. Weil, S. M. Chérif, A. Stashkevich, V. Jacques, A. Thiaville, and S. Rohart, *Nature Communications* **8**, 15765 EP (2017).
- [32] A. Neubauer, C. Pfleiderer, B. Binz, A. Rosch, R. Ritz, P. G. Niklowitz, and P. Böni, *Phys. Rev. Lett.* **102**, 186602 (2009).
- [33] I. Dzyaloshinsky, *Journal of Physics and Chemistry of Solids* **4**, 241 (1958).
- [34] T. Moriya, *Phys. Rev.* **120**, 91 (1960).
- [35] G. E. Volovik, *Journal of Physics C: Solid State Physics* **20**, L83 (1987).
- [36] J. Ye, Y. B. Kim, A. J. Millis, B. I. Shraiman, P. Majumdar, and Z. Tešanović, *Phys. Rev. Lett.* **83**, 3737 (1999).
- [37] K. Ohgushi, S. Murakami, and N. Nagaosa, *Phys. Rev. B* **62**, R6065 (2000).
- [38] N. Kanazawa, Y. Onose, T. Arima, D. Okuyama, K. Ohoyama, S. Wakimoto, K. Kakurai, S. Ishiwata, and Y. Tokura, *Phys. Rev. Lett.* **106**, 156603 (2011).
- [39] T. Kurumaji, T. Nakajima, M. Hirschberger, A. Kikkawa, Y. Yamasaki, H. Sagayama, H. Nakao, Y. Taguchi, T.-h. Arima, and Y. Tokura, *ArXiv e-prints* (2018), 1805.10719.
- [40] T. Okubo, S. Chung, and H. Kawamura, *Phys. Rev. Lett.* **108**, 017206 (2012).
- [41] A. O. Leonov and M. Mostovoy, *Nature Communications* **6**, 8275 EP (2015).
- [42] I. Martin and C. D. Batista, *Phys. Rev. Lett.* **101**, 156402 (2008).
- [43] Y. Kato, I. Martin, and C. D. Batista, *Phys. Rev. Lett.* **105**, 266405 (2010).
- [44] A. Chacon, L. Heinen, M. Halder, A. Bauer, W. Simeth, S. Mühlbauer, H. Berger, M. Garst, A. Rosch, and C. Pfleiderer, *Nature Physics* **14**, 936 (2018).
- [45] I. A. Ado, A. Qaiumzadeh, R. A. Duine, A. Brataas, and M. Titov, *Phys. Rev. Lett.* **121**, 086802 (2018).
- [46] A. Qaiumzadeh, I. A. Ado, R. A. Duine, M. Titov, and A. Brataas, *Phys. Rev. Lett.* **120**, 197202 (2018).
- [47] J. Rowland, S. Banerjee, and M. Randeria, *Phys. Rev. B* **93**, 020404 (2016).
- [48] A. O. Leonov, *ArXiv e-prints* (2014), 1406.2177.
- [49] P. W. Anderson and H. Hasegawa, *Phys. Rev.* **100**, 675 (1955).
- [50] K. Hamamoto, M. Ezawa, and N. Nagaosa, *Phys. Rev. B* **92**, 115417 (2015), 1504.06024.
- [51] B. Göbel, A. Mook, J. Henk, and I. Mertig, *Phys. Rev. B* **95**, 094413 (2017).
- [52] B. Göbel, A. Mook, J. Henk, and I. Mertig, *New Journal of Physics* **19**, 063042 (2017).
- [53] S. Hayami, S.-Z. Lin, and C. D. Batista, *Phys. Rev. B*

- 93**, 184413 (2016).
- [54] D. R. Hofstadter, Phys. Rev. B **14**, 2239 (1976).
- [55] A. H. MacDonald, Phys. Rev. B **28**, 6713 (1983).
- [56] N. Nemeč and G. Cuniberti, Phys. Rev. B **75**, 201404 (2007).
- [57] R. Bistritzer and A. H. MacDonald, Phys. Rev. B **84**, 035440 (2011).
- [58] C. R. Dean, L. Wang, P. Maher, C. Forsythe, F. Ghahari, Y. Gao, J. Katoch, M. Ishigami, P. Moon, M. Koshino, et al., Nature **497**, 598 (2013).
- [59] L. A. Chizhova, F. Libisch, and J. Burgdörfer, Phys. Rev. B **90**, 165404 (2014).
- [60] D. Weiss, K. von Klitzing, K. Ploog, and G. Weimann, Surface Science **229**, 88 (1990).
- [61] D. Weiss, A. Menshig, K. von Klitzing, and G. Weimann, Surface Science **263**, 314 (1992).
- [62] C. Albrecht, J. H. Smet, K. von Klitzing, D. Weiss, V. Umansky, and H. Schweizer, Phys. Rev. Lett. **86**, 147 (2001).
- [63] M. C. Geisler, J. H. Smet, V. Umansky, K. von Klitzing, B. Naundorf, R. Ketzmerick, and H. Schweizer, Phys. Rev. Lett. **92**, 256801 (2004).
- [64] In each Pd/Si layer, the Pd and Si atoms could form a superstructure with a quadrupled unit cell (see Ref. [31]). We find this leads to bond-dependent DM interactions, but with DM vectors which *spatially average to zero*. For simplicity, we ignore such spatially varying DM terms, and instead assume a homogeneous random configuration or a short-correlation length superstructure for the Pd and Si atoms. Inversion is then recovered on average, so the DM term can be ignored. However, we retain the compass anisotropy which is symmetry-allowed (even when inversion symmetry is present) and appears to be important for magnetism in Gd₂PdSi₃.